Research Article ISSN: 2349 – 7106

Asian Journal of Research in Chemistry and Pharmaceutical Sciences

Journal home page: www.ajrcps.com

https://doi.org/10.36673/AJRCPS.2023.v11.i02.A11

FABRICATION, MORPHOLOGICAL, OPTICAL, CONDUCTING AND GAS SENSING BEHAVIOR OF Zn-Mn-Al_2O_3 DOPED POLYPYRROLE NANO COMPOSITES

Earamma*[1] and Nirdosh Patil[1]

[1*]Department of Chemistry, Sharnbasva University, Kalaburagi-585103, Karnataka, India.

ABSTRACT

Zn-Mn-Al_2O_3 pervoskite was doped in polypyrrole solution in accordance to weight percentage composition of 5%, 10%, 15%, 20%, and 25% by a two-step method via wet impregnation method at ambient temperature resulted in Zn-Mn-Al_2O_3 doped polypyrrole nano composite thin films are conductive and porous. The Zn-Mn-Al_2O_3 /PPy was being characterized using various methods. Thin films generated, comprising of two-probe electrical resistivity, scanning electron microscopy (SEM), Fourier transform infrared (FTIR) spectroscopy, and X-ray diffraction. The structural formation of Zn-Mn-Al_2O_3 /polypyrrole was determined using FTIR, XRD, and SEM investigations. All thin films have shown decrease in electrical resistivity as concentration of Zn-Mn-Al_2O_3 increases as dopant with polypyrrole, which indicates higher conductivity of thin films with Zn-Mn-Al_2O_3 as a dopant. Surface morphology of Zn-Mn-Al_2O_3/polypyrrole materials has been discovered substantial influence on the thermal stability and the ability to detect gases. All the thin films were studied for the H_2S gas sensing behavior. The antimicrobial and antifungal activities of the investigated PPy and its PPy/Zn-Mn-Al_2O_3 nanocomposite materials using the cup plate technique at various doses in DMSO solvent using the minimum inhibitory concentration (MIC) method. The antimicrobial study indicates that its PPy/Zn-Mn-Al_2O_3 (20%) and PPy/Zn-Mn-Al_2O_3 (25%) have high microbial activity, whereas PPy has moderate activity as compared to standard.

KEYWORDS

Polypyrrole, Metal oxide, Monomer and Aluminate.

Author for Correspondence:

Earamma,

Department of Chemistry,

Sharanbasva University,

Kalaburagi, Karnataka, India.

Email: ramamallikarjun@gmail.com

INTRODUCTON

High electrical conductivity, stable environment, simplicity in obtaining as well as biocompatibility, the monomer are just a few of the meritorious characteristics of polypyrrole, a highly desired conjugated polymer, which has been the subject of thorough investigation in both its bulk and thin film forms[1]. Pyrrole is a straightforward heterocyclic organic monomer. Kanazawa and colleagues were the first to recognize polypyrrole (PPy) as an electrical conductor, and the electrochemical oxidation of pyrrole was used as the production method[2]. Although this material's polymerized form has been the subject of extensive research, nothing is known about its electrical transport characteristics. The majority of research on polypyrrole that has been published relies on its electrochemically produced version. There have been several findings on polypyrrole's ionic conductivity and charge transfer mechanism[3]. In its PF_6 doped form, polypyrrole has a dc electrical conductivity that ranges from 200 to 500S/cm and is dependent on temperature, preparation circumstances and the type of do pants used. Also reported in polypyrrole[4] are the metal insulator transition and disorder-induced charge localization.

Due to their affordability, ease of Synthesis is also convenience of electronic measurement methods, metal oxides such as In_2O_3[5,6] Fe_2O_3[7,8] In addition to CuO[9,10] ZnO[11], SnO_2[12-14] and Ga_2O_3[15], widely researched to detect different chemicals. Ga_2O_3 is a wide-band gap n-type semiconductor. That has been extensively researched for use in solar cells, optical electronics, gas sensors, and catalysts, among other things[16,17]. Ga_2O_3 was typically used gas monitors for high temperatures before this work owing to its chemical and thermal resilience. According to Baban and others[18], rf magnetron sputtered Ga_2O_3 thin films were capable of detecting oxygen at 100°C. Fleischer and colleagues used the sputter method to make the Ga_2O_3 H_2S is detected in thin films at 400-650°C[19]. Nevertheless, an elevated working temperature results in a complex sensor measurement system and considerable energy usage. According to studies, metal oxide/carrier composites, Metal oxide/carbon nanomaterial compounds, binary metal oxide semiconductor (BMO) materials, and noble metal/metal ox-ide composite materials can all enhance methane detection capability[20-26]. Among these methods, putting on-board active gas-sensing components affordable transporters of plenty of holes and a big a particular surface region both significantly lower the cost and effectively increase gas-sensing performance. Al_2O_3 is one of the most promising alternatives among a range of carriers because of its inexpensive cost, abundant channels, and substantial specific surface area[27]. For the oxidation of toluene, Gan et al. created an Al_2O_3 supported-Pt catalyst and they investigated the synergistic effects in the catalytic mechanism of the Al_2O_3 carrier and Pt nanoparticles[28].

EXPERIMENTAL

Materials

Metal oxide nano composites were created using aluminium isopropoxide, glucose, zinc acetate ($Zn(CH_3COO)_2$) and $MnCl_24H_2O$, all of which were purchased from S.D. Fine Chemicals in India. Pyrrole monomer with ammonium persulfate (mPPy) (Sigma-Aldrich, USA). All of the aqueous solutions for the synthesis were made with deionized water and a straightforward wet impregnation procedure.

Preparation of polypyrrole

The chemical oxidative polymerization method was used to create polypyrrole (PPy) by mixing pyrrole and hydrochloride acid in an equal amount (0.1M) in a liquid the medium, then the adding of ammonium persulfate (0.2M) drop by drop at 0-50°C for 12 hours in a cold bath. The procedure of polymerization was carried out for six hours with steady stirring. The polypyrrole precipitate was obtained after a day via filtration and frequently washed with an ethanol mix and distilled water. Then it dried in the air for 24 hours at 60°C prior to being turned into a powder.

Preparation of Zn-Mn-Al_2O_3

Supplementary Material contains information on all chemicals (Text S1). To Deionized water, 60ml, add aluminium zinc acetate, dextrose, and isopropoxide $Zn(CH_3COO)_2$ and $MnCl_24H_2O$ in a specific ratio. 360 minutes of vigorous stirring in a 60°C water plunge, then change the water solution's pH to 5and stir again for 300 minutes to fully combine. At 100°C, the combined fluid was dried, after being left to remain for the night. To create the dried substance was heated to 600°C at a rate of 5°C/min in a muffle furnace to produce the Zn and Mn doped Al_2O_3 precursor.

Preparation of Zn-Mn-Al_2O_3/Polypyrrole composite thin films

Deionized water was used to dissolve polypyrrole (PPy) at 90°C before it was reduced to 10 wt%. The polypyrrole solution was combined with the Zn-Mn-Al_2O_3 powder after being further pulverised to a size smaller than 50nm. A Teflon petridish was used to cast the homogeneous slurry, which then solidified at room temperature, creating a formation barrier with an extent of between 0.2 and 0.5nm. Then, the barrier desiccated for 24 hours at 60°C before being kept in a dry environment. Different PPy-Zn-Mn-Al_2O_3 composites were created using the wet impregnation method by doping various Zn-Mn-Al_2O_3 compositions (5, 10, 15, 20 and 25%) into a polypyrrole water solution.

RESULTS AND DISCUSSION

X-ray energy-dispersive spectroscopy (EDS)

Zn, Mn, Al, C, and N atoms are dispersed in Zn-Mn-Al_2O_3 and polypyrrole according to the measurement of energy dispersive X-ray spectroscopy of this material respectively (Figure No.1a and Figure No.1b). Al_2O_3 is represented by the (311), (400), (511), (440) and (220) crystal planes in XRD (Figure No.1c)[19,20]. The diffraction peaks of Al_2O_3 shifted to low angles due to the Zn and Mn poisoning, but no new peaks emerged, further demonstrating the doping of into the Zn and Mn. Al_2O_3 diamond composition. Polypyrrole is responsible for the apex at 27.8. (002). This suggests that the surface contains polar aromatic rings of Zn-Mn-Al_2O_3, which can result in aromatic compounds' electron donors interacting with donors, increasing the binding of aromatic compounds[21,22]. The various Zn-Mn-Al_2O_3 compositions (5, 10, 15, 20 and 25%) into an aqueous solution of polypyrrole samples shown in EDX that increases the broadness in the peaks of as weight percentage of Zn-Mn-Al_2O_3 do pants decreases in PPy, It is also observed that there is a slight shift of all the peaks to lower angles indicate that the dispersion of Zn-Mn-Al_2O_3 into the PPypolymer.

FTIR

Al-O vibration is responsible for the recognisable peak at 556cm^{-1} (Figure No.2)[23]. The distinctive high point of Al-O moves to a high wave number after Zn and Mn doping. This suggests the extent of the Al-O bond in Zn-Mn-Al_2O_3 shortens, possibly as a result of the alteration in Al-O covalent. The O-H bond's tensile vibration and bending vibration on the surface of Al_2O_3 are represented by the characteristic peaks at 3463cm^{-1} and 1635.9cm^{-1}, respectively[24]. The O-H bond on the Al_2O_3 surface experiences tensile vibration and bending vibration, respectively, as indicated by the distinctive peaks at 3463cm^{-1} and 1635.9cm^{-1}. Water adsorption peaked at the polypyrrole surface, according to published sources[20,25,26], is around 3156cm^{-1}. The height of that the deposition of Zn-Mn-Al_2O_3 on polypyrrole polymer layer. It is observed that the disappearance of the peak at 3440cm^{-1} in all doped Zn-Mn-Al_2O_3 polypyrrole (Ppy/Zn-Mn-Al_2O_3) composite materials

Morphology study using SEM

Figure No.3 displays the combined films' SEM images formed of PPy /Zn-Mn-Al_2O_3 and Zn-Mn-Al_2O_3. The microstructures of the doped and undoped samples may be distinguished with clarity by the SEM. polypyrrole that hasn't been doped generally has a more granular structure than one that has. When do pants were used in the polymerization with polypyrrole, it was found that the granule sizes varied. The morphology of the PPy /Zn-Mn-Al_2O_3 films is entirely distinct from that of the doped polypyrrole. For illustration, as shown in Figure No3, the microscopic Zn-Mn-Al_2O_3, the combination of particles that spread into the PPy layer results in semi-spherical structures called grains, comprehensive investigation of the SEM may also reveal the appearance the presence of microscopic the microstructures contain fissures or voids. Polypyrrole/Zn-Mn-Al_2O_3 composites that are indicative of similar gaps appearing in relation to the change from order to chaos in Zn-Mn-Al_2O_3, as seen by S. A. El All[27]. It is believed that these morphological traits are advantageous for uses involving gas sensing.

Optical properties

The visual attributes of Zn-Mn-Al_2O_3, and PPy /Zn-Mn-Al_2O_3, samples analysed between 300 and 1800nm, optical transmission (T) bands are displayed in Figure 4(a). As photon dispersion increases brought on by the produced Increasing photon scattering is what is responsible for the lower the videos' transmission with higher Zn-Mn-Al_2O_3, doping concentrations[28]. Figure No.4 the optical absorption index is displayed (α) of PPy /Zn-Mn-Al_2O_3, movies with a variety Zn-Mn-Al_2O_3, Doping substances (b). Beer-law the following is how Lambert's[29] estimates the absorption coefficient:

$$\alpha = \ln(1/T)(1/d)$$

Where d is the fabric's width sheet and T is the transmittance. The thickness of a layer without polypyrrole/Zn-Mn-Al_2O_3 is 445nm, while films doped with different concentrations of Zn-Mn-Al_2O_3 are 465 nm thick. It has been discovered that as the Zn-Mn-Al_2O_3 proportion grows, the wavelength (λ) decreases while the (α) increases. The explicit permitted band gap for energy (Eg) of PPy/Zn-Mn-Al_2O_3 specimens have been calculated using the relationship between the absorption coefficient (α) and the incoming photon energy (h).

$\alpha h\nu = A(h\nu\text{-}Eg)n$

The measurement of the optical band gap (Eg) was calculated, as seen in Figure No.4b, by extending the straight line of the curve section to the (h) axis[30]. The findings demonstrate that the optical band gap increases along with increasing Zn-Mn-Al_2O_3 doping levels, which is compatible with variations in particle size. The impact of Burstein-Moss on band gap widening, a well-known quantum confinement event, resulting in the band separation widen both when the amount of doping is increased and when the particle size is decreased[31,32]. The spread of mid-level energy levels in the voids of the band may also change as a result of structural disturbance in the lattice, affecting the Eg values. The increase in Eg indicates that optoelectronic components might use polypyrrole/Zn-Mn-Al_2O_3 films. The proportion called the and polypyrrole/Zn-Mn-Al_2O_3 material expanded.

Electrical conductivity measurement

As shown in Table No.1, the conductivity of polypyrrole and the level of doping in the pelletized powder samples is only slightly lower than that of the polypyrrole films formed from the solvents. This is resulting from the various structural flaws that can occur in polypyrrole strands that can seriously affect the flow of charge carriers and in turn, the conductivity of the polymer. Since anionic surfactants change the polypyrrole chains' conducting network and add an ordered collection of macromolecular chains, adding them to the polymer's backbone will increase conductivity[33].

Gas Sensor

For the purpose of detecting H_2S gas, the entire Zn-Mn-Al_2O_3 quantities of doped polypyrrole were analysed. Figure No.5 depicts a representative histogram of polypyrrole's current over time produced after the presence of H_2Svapour.

To evaluate the consistency of mechanisms of adsorption and desorption of the samples, each sample was tested three times. The second and third rounds' current (I) vs. time graphs may be seen in Figure No.5 to vary somewhat from the initial cycle. This can be the case since the procedure of desorption wasn't finished in the allotted period.

Equation is used to determine the sensitivity factor.

$$S = \frac{Rg - Ro}{Ro}$$

Where Rg and Ro, respectively, resistances in gaseous and gasless air[34,35]. The results of it is being looked into calculations for ammonia gas and Zn-Mn-Al_2O_3 doped polypyrrole sensors made utilizing various fabrication techniques.

It was demonstrated that various the components reacted to H_2S gas in distinct methods for pure and polypyrrole and polypyrrole filled with polypyrrole/Zn-Mn-Al_2O_3. These experiments showed that when H_2S the gas was released Zn-Mn-Al_2O_3 doped polypyrrole which had been injected with various percentages of weight Zn-Mn-Al_2O_3 do pants, a decrease in current was seen. Greater than unadulterated electrical conductivity polypyrrole is a sign that the Zn-Mn-Al_2O_3 doping process generated a sizable number charged transporters with heavy doping. Because of the higher charge density, H_2S cannot generate additional charges; instead, it reduces the effective charge. Polypyrrole's conductivity will therefore decrease in this situation, as has actually been observed in our study.

Antimicrobial activities

The antimicrobial activities (antibacterial and antifungal activities) of all Zn-Mn-Al_2O_3 doped PPy nanocomposite materials at different concentrations of Zn-Mn-Al_2O_3 with PPy in DMSO solvent by minimum inhibitory concentration (MIC) method. Antibacterial activity against *Escherichia Coli* and *Staphylococcus Aureus* were evaluated and antifungal activity against *Aspergillusniger* and *Cladosporium* were evaluated, Gentamycine and fluconazole common antibiotics were also evaluated for antimicrobial and antifungal activity at the same proprtion as the Zn-Mn-Al_2O_3 doped PPy nanocomposite materials under the same conditions.

The results (Table No.3) demonstrate that the PPy/Zn-Mn-Al_2O_3 (25%) have high bacterial and fungal activity, which is attributed to the PPy/Zn-Mn-Al_2O_3 (25%) quicker diffusion[24,25], while the PPy has moderate activity.

Table No.1: Transmission of electricity in polypyrrole and doped polypyrrole samples in an encapsulated state

Initial No	Initial Example	S/cm Conductivity
1	Polypyrrole	2.40×10^{-3}
2	PPy /Zn-Mn-Al_2O_3 (10%)	12.22×10^{-2}
3	PPy /Zn-Mn-Al_2O_3 (15%)	15.12×10^{-2}
4	PPy /Zn-Mn-Al_2O_3 (20%)	18.62×10^{-2}
5	PPy /Zn-Mn-Al_2O_3 (25%)	25.62×10^{-2}

Table No.2: Conducting polymers / metal oxides doped composites used in H2S gas sensors

S.No	Iron oxalate	Polymer	Concen (ppm)	Response	Reaction and recuperation times (s)	T(^{o}C)	References
1	Au	PANI	1	0.05	--	RT	36
2	Ag	PANI	10	100	360	RT	37
3	TiO_2	PPy	50	4	--	--	38
4	$CuSnO_2$	PPy	50	89	--	RT	39
5	WO_3	PT	100	1.35	<15	70	40
6	PPy/Zn-Mn-Al_2O_3 (10%)	PPy	100	73	--	RT	Present Study
7	PPy/Zn-Mn-Al_2O_3 (15%)	PPy	100	81	--	RT	Present Study
8	PPy/Zn-Mn-Al_2O_3 (20%)	PPy	100	88	--	RT	Present Study
9	PPy/Zn-Mn-Al_2O_3 (25%)	PPy	100	83	--	RT	Present Study

Table No.3: The antimicrobial activity of PPy and its PPy/Zn-Mn-Al_2O_3 nanocomposite materials evaluated by (mm)

S.No	Samples	Zone of inhibition in mm			
		Antibacterial activity		Antifungal activity	
		Escherichia Coli	*Staphylococcus Aureus*	*Aspergillus Niger*	*Cladosporium*
1	PPy	15	16	17	14
2	PPy/Zn-Mn-Al_2O_3 (5%)	21	23	26	21
3	PPy/Zn-Mn-Al_2O_3 (10%)	23	14	22	24
4	PPy/Zn-Mn-Al_2O_3 (15%)	24	22	24	22
5	PPy/Zn-Mn-Al_2O_3 (20%)	24	24	25	26
6	PPy/Zn-Mn-Al_2O_3 (25%)	25	27	28	27
7	Gentamycine	27	29	-	-
8	Fluconazole	-	-	30	25

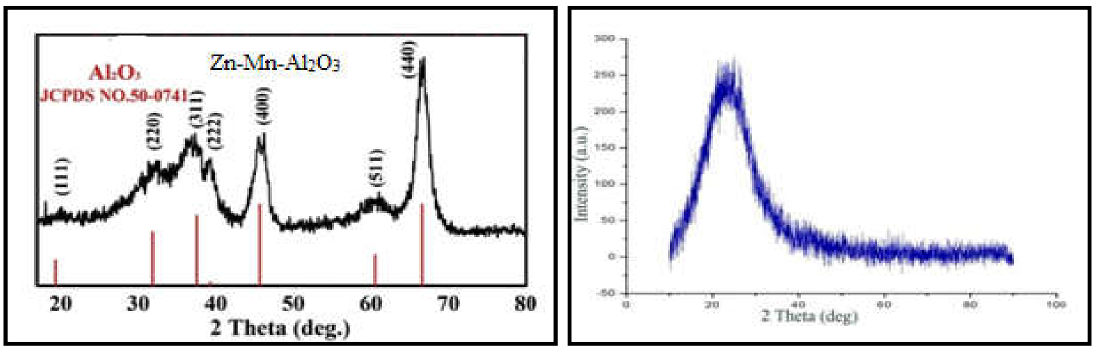

Figure No.1a: XRD patterns of Zn-Mn-Al_2O_3 (b). XRD patterns of polypyrrole

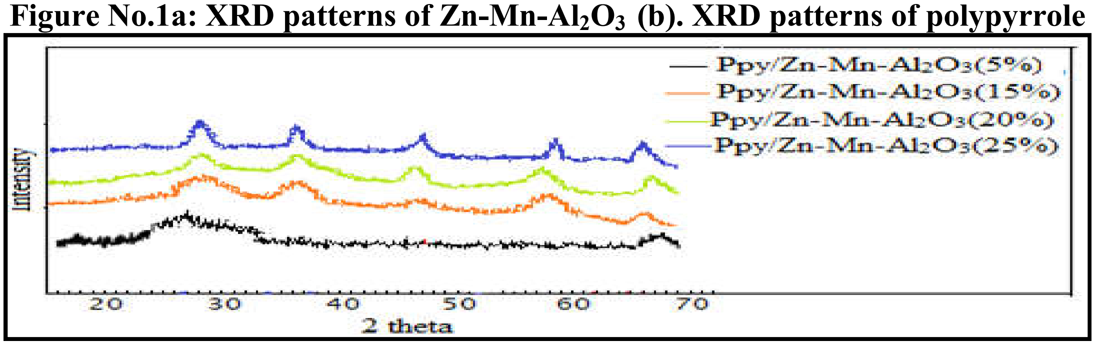

Figure No.1c: XRD patterns of PPy/Zn-Mn-Al_2O_3 patterns of different concentrations

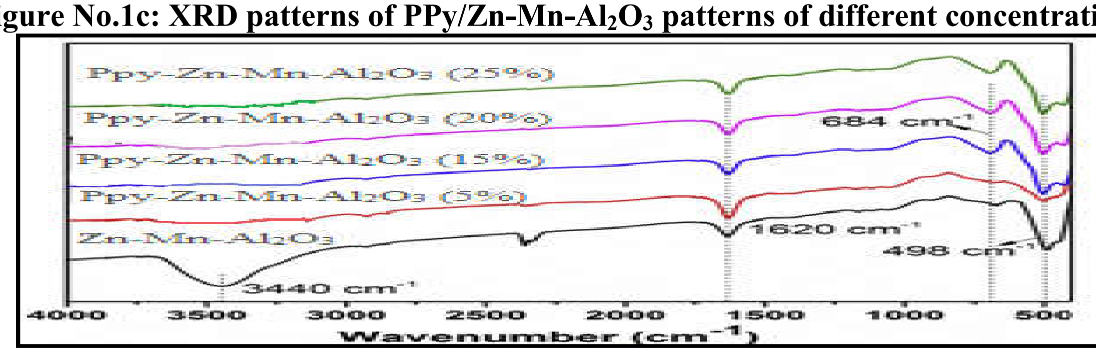

Figure No.2: Fourier transform infrared (FTIR) spectra of the Zn-Mn-Al_2O_3 and Zn-Mn-Al_2O_3 doped (5, 15, 20 and 25 wt%) to polypyrrole

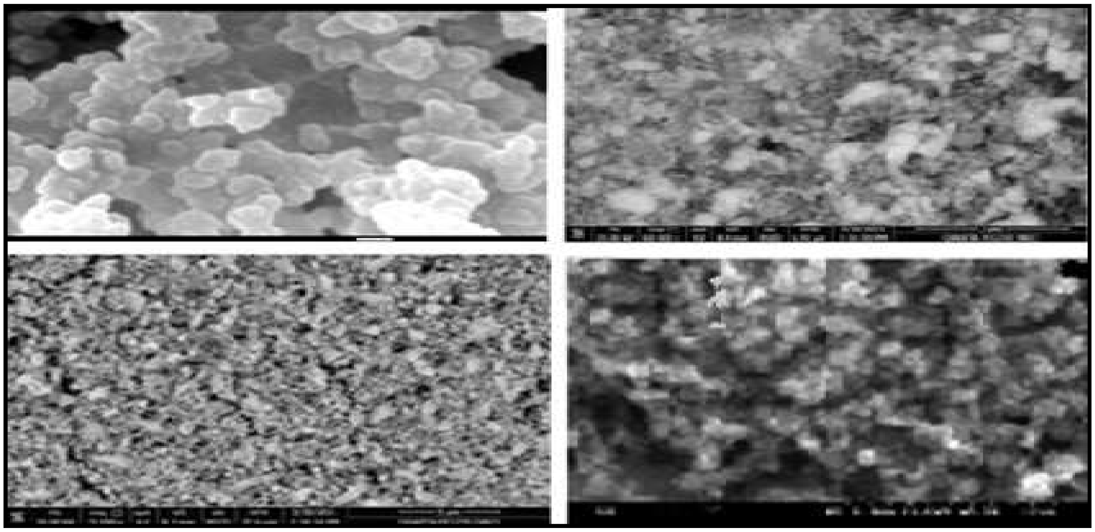

Figure No.3: SEM images of PPy/Zn-Mn-Al_2O_3 of varying concentrations

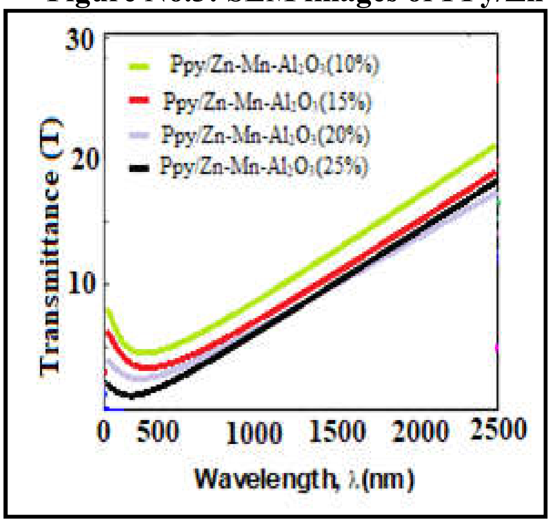

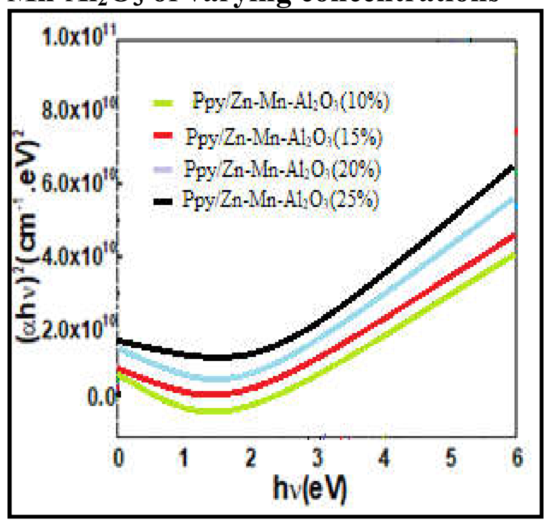

Figure No.4a: Transmission and frequency correlation (nm) **Figure No.4b: (αhν)2 versus hν (eV)**

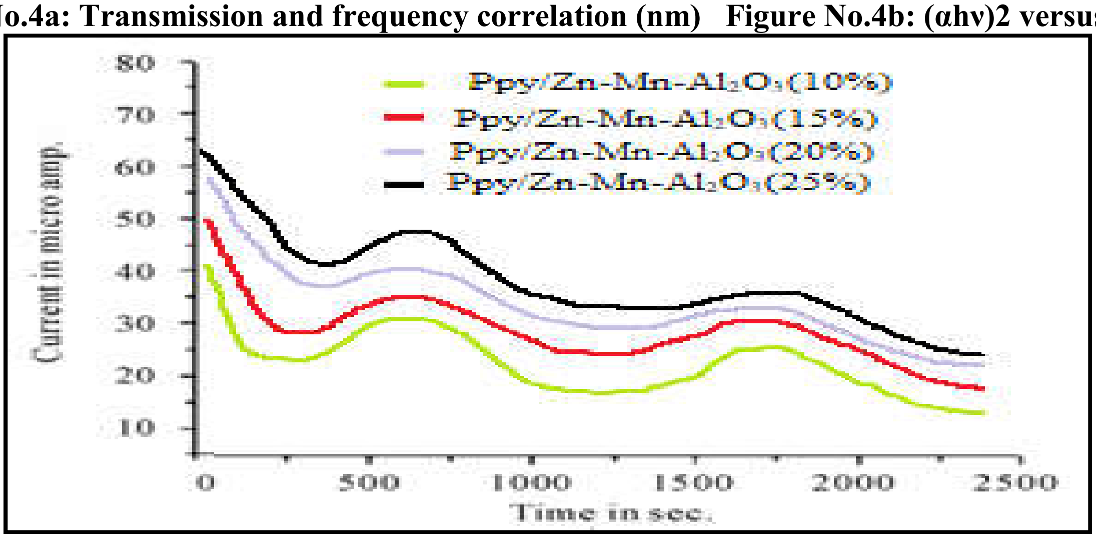

Figure No.5: The reaction from various PPy /Zn-Mn-Al_2O_3 examples of towards H_2S gas

CONCLUSION

PPy/Zn-Mn-Al_2O_3Chemical oxidation was used to create thin sheets made of polymer nanocomposite materials. These significant changes stem from a molecular interaction between Polypyrrole and Zn-Mn-Al_2O_3 nanoparticles observed in IR spectra of PPy/ Zn-Mn-Al_2O_3. The O-H bond on the Al_2O_3 surface experiences tensile vibration and bending vibration, respectively, as indicated by the distinctive peaks at 3463cm^{-1} and 1635.9cm^{-1}. About 3156cm^{-1} of water has been adsorbed at its apex on the polypyrrole surface. About 3500cm^{-1} is the height of the water pinnacle adsorbed on the metal oxide. The IR spectroscopy of PPy/Zn-Mn-Al_2O_3 therefore shows that there is no peak at 3156cm^{-1} and at 3463cm^{-1}, respectively. This demonstrates the deposition of Zn-Mn-Al_2O_3 on polypyrrole polymer layer. An XRD analysis shows that the Zn-Mn-Al_2O_3 doped polypyrrole diffraction peaks become stronger after being inserted into the structure of polypyrrole, showing the well-crystalline nature of the resulting PPy/Zn-Mn-Al_2O_3composite films. The XRD design also indicated which the sharpness among the summits increased with dopant (Zn-Mn-Al_2O_3) percentage, which caused composite materials to transform from as a dopant, amorphous to solid (Zn-Mn-Al_2O_3) concentration increased in the Matrix of polypyrrole. The PPy/Zn-Mn-Al_2O_3 composite's microstructures exhibit tiny cavities or dark holes, which the SEM shows are comparable in order for such holes to develop linked with the shift from order to disorder in Zn-Mn-Al_2O_3. All samples' optical characteristics were investigated in the 300-600nm wavelength region to 1800nm. The findings demonstrate that the optical band gap rises with increasing Zn-Mn-Al_2O_3 doping levels, what is commensurate with modifications to particulate size. The determination of conductivity shows that adding Zn-Mn-Al_2O_3 to the core of the polypyrrole network will increase conductivity because it modifies the conducting network of the link. For the purpose of detecting H_2S gas, all the Zn-Mn-Al_2O_3 doped polypyrrole samples were investigated. The observation was made that dopant (Zn-Mn-Al_2O_3) concentration levels rise the reaction of the composites made of polypyrrole and Zn, Mn, and Al_2O_3 also improved. The antimicrobial and antifungal activities of the investigated PPy and its PPy/Zn-Mn-Al_2O_3nanocomposite materials using the cup plate technique at various doses in DMSO solvent using the minimum inhibitory concentration (MIC) method. The research indicates that its PPy/Zn-Mn-Al_2O_3 (20%) and PPy/Zn-Mn-Al_2O_3 (25%) have high microbial activity, whereas PPy has moderate activity as compared to standard.

ACKNOWLEDGEMENT

The authors are thankful to Poojya Dr. Sharanabasawappa Appa, President Sharnabasveshwar Vidya Vardhak Sangha, Kalaburagi, Registrar Dr. Anilkumar Bidve and Dean Dr. Laxmi Patil of Sharnbasva University, Kalaburagi, for encouragement during the process of Carrying out this work.

CONFLICT OF INTEREST

We declare that we have no conflict of Interest.

BIBLIOGRAPHY

1. Ju E, Sik K, Macdiarmid A G. High molecular weight soluble polypyrrole, *Synth. Met,* 125(3), 2002, 267-272.
2. Terje A. Skotheim. Handbook of conducting polymers, *Marcel Decker, Inc, New York, Chapter 14,* 1986.
3. Yoon C O, Reghu M, Moses D, Heeger A J. Transport near the metal-insulator transition: Polypyrrole doped with PF_6, *Phys. Rev. B,* 49(16), 1994, 10851.
4. Chapman B, Buckley R G, Kemp N T, Kaiser A B, Beaglehole D, Trodahl H J. Low-energy conductivity of PF_6-doped polypyrrole, *Phys. Rev. B,* 60(19), 1999, 13479.
5. Han D, Zhai L, Gu F. Highly sensitive NO_2 gas sensor of ppb-level detection based on In_2O_3 nanobricks at low temperature, *Sens. Actuators, B,* 262, 2018, 655-663.
6. Xiao B, Wang D, Song S. Fabrication of meso- porous In_2O_3nanospheres and their ultrasensitive NO_2 sensing properties, *Sens. Actuators B,* 248, 2017, 519-526.

7. Liu C, Wang Y, Zhao P, Li W, Wang Q, Sun P, Chuai X, Lu G. Porous a-Fe_2O_3microflowers: Synthesis, structure and enhanced acetone sensing performances, *J. Colloid Interface Sci,* 505, 2017, 1039-1046.
8. Jin C, Ge C, Xu G, Peterson G, Jian Z, Wei Y, Zhu K. Influence of nanoparticle size on ethanol gas sensing performance of mesoporous a-Fe_2O_3 hollow spheres, *Mater. Sci. Eng. B,* 224, 2017, 158-162.
9. Wang H, Yan L, Li S, Li Y, Liu L, Du L, Duan H, Cheng Y. Acetone sensors based on microsheet-assembled hierarchical Fe_2O_3 with different Fe^{+3} concentrations, *Appl. Phys. A,* 124(2), 2018, 212.
10. Kim M J, Lee S, Lee K M, Jo H, Choi S S, Lee Y S. Effect of CuO introduced on activated carbon fibers formed by electroless plating on the NO gas sensing, *J. Ind. Eng. Chem,* 60, 2018, 341-347.
11. Oosthuizen D N, Motaung D E, Swart H C. In depth study on the notable room-temperature NO_2 gas sensor based on CuO nanoplatelets prepared by sonochemical method: Comparison of various bases, *Sens. Actuators, B,* 266, 2018, 761-772.
12. Zhou X, Wang A, Wang Y, Bian L, Yang Z, Bian Y, Gong Y, Wu X, Han N, Chen Y. Crystal-defect-dependent gas-sensing mechanism of the single ZnO nano wire sensors, *ACS Sens,* 3(11), 2018, 2385-2393.
13. Chen Y, Qin H, Cao Y, Zhang H, Hu J. Acetone sensing properties and mechanism of SnO_2 thick-films, *Sensors,* 18(10), 2018, 3425.
14. Vorokhta M, Khalakhan I, Vondracek M, Tomecek D, Vorokhta M, Maresova E, Novakova J, Vlcek J, Fitl P, Novotny M, Hozak P, Lancok J, Vrnata M, Matolinova I, Matolin V. Investigation of gas sensing mechanism of SnO_2 based chemiresistor using near ambient pressure XPS, *Surf. Sci,* 677(1-10), 2018, 284e-290.
15. Xu L, Zeng W, Li Y. Synthesis of morphology and size-controllable SnO_2 hierarchical structures and their gas-sensing performance, *Appl. Surf. Sci,* 457, 2018, 1064-1071.
16. Mazeina L, Bermudez V M, Perkins F K, Arnold S P, Prokes S M. Interaction of functionalized Ga_2O_3 NW-based room temperature gas sensors with different hydrocarbons, *Sens. Actuators, B,* 151(1), 2010, 114-120.
17. Pearton S J, Yang J, Cary P H, Ren F, Kim J, Tadjer M J, Mastro M A. A review of Ga_2O_3 materials, processing and devices, *Appl. Phys. Rev,* 5, 2018, 1-57.
18. Mohammadi M R, Fray D J. Semiconductor TiO_2-Ga_2O_3 thin film gas sensors derived from particulate sol-gel route, *Acta Mater,* 55(13), 2007, 4455-4466.
19. Baban C, Toyoda Y, Ogita M. Oxygen sensing at high temperatures using Ga_2O_3 films, *Thin Solid Films,* 484(1), 2005, 369-373.
20. Fleischer M, Giber J, Meixner H. H_2-induced changes in electrical conductance of b-Ga_2O_3 thin-film systems, *Appl. Phys. A,* 54(6), 1992, 560-566.
21. Kim H, Jin C, An S, Lee C. Fabrication and CO gas-sensing properties of Pt-functionalized Ga_2O_3 nanowires, *Ceram. Int,* 38(5), 2012, 3563-3567.
22. Zhang S, Yang M, Liang K, Turak A, Zhang B, Meng D, Wang C, Qu F, Cheng W, Yang M. An acetone gas sensor based on nanosized Pt-loaded Fe_2O_3 nanocubes, *Sens. Actuators, B,* 290, 2019, 59-67.
23. Qu F, Shang W, Thomas T, Ruan S, Yang M. Self-template derived $ZnFe_2O_4$ double-shell microspheres for chemresistive gas sensing, *Sens. Actuators, B,* 265, 2018, 625-631.
24. Park S, Kim S, Sun G J, Lee C. Synthesis, structure and ethanol sensing properties of Ga_2O_3-core/WO_3-shell nanostructures, *Thin Solid Films,* 591(B), 2015, 341-345.
25. Dang L, Zhang G, Kan K, Lin Y, Bai F, Jing L, Shen P, Li L, Shi K. Hetero-structured Co_3O_4/PEI-CNTs composite: Fabrication, characterization and CO gas sensors at room

temperature, *J. Mater. Chem,* 2(13), 2014, 4558-4565.

26. Wang C, Yin L, Zhang L, Xiang D, Gao R. Metal oxide gas sensors: Sensitivity and influencing factors, *Sensors,* 10(3), 2010, 2088-2106.
27. El All S A, El-Shobaky G A. Structural and electrical properties of c-irradiated TiO_2/Al_2O_3 composite prepared by sol-gel method, *J. Alloy. Compd,* 479(1-2), 2009, 91-96.
28. Muiva C M, Sathiaraj T S, Maabong K. Effect of doping concentration on the properties of aluminium doped zinc oxide thin films prepared by spray pyrolysis for transparent electrode applications, *Ceram. Int,* 37(2), 2011, 555-560.
29. Swinehart D F. The beer-lambert law, *J. Chem. Educ,* 39(7), 1962, 333.
30. Gad S A, Shaban H, Mansour B A, Mahmoud G M. Determination and analysis of linear and nonlinear optical properties and electrical conductivity of amorphous PbxGe42-xSe48Te10 thin films, *Appl. Phys. A,* 126(5), 2020, 354.
31. Omran Alkhayatt A H, Hussian S K. Fluorine highly doped nanocrystalline SnO_2 thin films prepared by SPD technique, *Mater. Lett,* 155, 2015, 109-113.
32. Li J, Liu X. Preparation and characterization of a-MoO_3 nanobelt and its application in super capacitor, *Mater. Lett,* 112, 2013, 39-42.
33. Trchova M, Kova J. Synthesis and structural study of polypyrrole prepared in the presence of surfactants, *Synth. Met,* 138(3), 2003, 447-455.
34. Chitra P, Muthusamy A, Jayaprakash R. Structural, magnetic and dielectric properties of polyaniline /$MnCoFe_2O_4$ nano composites, *J. Magn. Magn. Mater,* 396, 2015, 113-120.
35. Sengupta P P, Barik S, Adhikari B, Polyaniline as a gas-sensor material, *Materials and Manufacturing Processes,* 21(3), 2007, 263-270.
36. Liu C, Hayashi K, Toko K. Au nanoparticles decorated polyanilinenanofiber sensor for detecting volatile sulfur compounds in expired breath, *Sensor Actuat B-Chem,* 161(1), 2012, 504-509.
37. Mekki A, Joshi N, Singh A, *et al*. H_2S sensing using in situ photo-polymerized polyaniline silver nano composite films on flexible substrates, *Org Electron,* 15(1), 2014, 71-81.
38. Hakimi M, Salehi A, Boroumand F A. Fabrication and characterization of an ammonia gas sensor based on PEDOT-PSS with N-doped graphene quantum dots do pant, *IEEE Sens J,* 16(16), 2016, 6149-6154.
39. Bai S, Zhang K, Sun J, *et al*. Polythiophene-WO_3 hybrid architectures for low-temperature H_2 S detection, *Sensor Actuat B-Chem,* 197, 2014, 142-148.
40. Antonio Vazquez-Lopez, Javier Bartolome, Ana Cremades, David Maestre. High-performance room-temperature conductometric gas sensors: Materials and strategies, *Chemosensors,* 10(6), 2022, 227.

Please cite this article in press as: Earamma and Nirdosh Patil. Fabrication, morphological, optical, conducting and gas sensing behavior of Zn-Mn-Al_2O_3 doped polypyrrole nano composites, *Asian Journal of Research in Chemistry and Pharmaceutical Sciences,* 11(2), 2023, 68-77.